Proceedings of the 2001 IEEE
International Conference on Robotics & Automation
Seoul, Korea - May 21-26, 2001

Robot Localization in Nonsmooth Environments: Experiments with a New Filtering Technique

Fabio M. Antoniali Giuseppe Oriolo
Dipartimento di Informatica e Sistemistica
Università di Roma "La Sapienza"
Via Eudossiana 18, 00184 Roma, Italy
{antonial,oriolo}@dis.uniroma1.it

Abstract

We consider the localization problem for a unicycle robot equipped with range finders and moving in environments with nonsmooth geometry, i.e., whose obstacle-free region has a piecewise-linear boundary. Using the Multi-Hypothesis Density Filter, a novel multi-modal estimator based on the bayesian framework, an innovative localization system is devised and implemented on the ATRV-Jr robot. Experiments illustrate the superior performance of the new filter with respect to the classical Extended Kalman filter.

1 Introduction

The subject of this paper is the localization problem for a mobile robot with unicycle kinematics, moving in a known 2D environment. The robot is assumed to be equipped with an exteroceptive sensory system consisting of a set of range finders, each measuring the distance along its direction between the robot and the obstacle region, made of walls and other objects.

Under the hypothesis that the boundary of the obstacle-free region can be described by piecewise-linear functions, the measurement model inherits the same non-smoothness property. To account for this peculiar (but realistic) circumstance, ignored by most localization systems, we introduce the Multi-Hypothesis Density Filter (MHDF), a nonlinear filter whose performance is improved over conventional unimodal estimators, such as the Extended Kalman Filter (EKF).

The structure of the MHDF is presented in Sect. 2. Assuming that a heading sensor is available, state and measurement models are derived in Sect. 3 and shown to satisfy the conditions required by the MHDF. In Sect. 4, we describe an implementation of the MHDF localization system on the ATRV-Jr mobile robot, and present comparative experiments w.r.t. an EKF-based system. These show that the MHDF provides remarkably better localization performance than the EKF.

2 Multiple-Hypothesis Density Filter

A short description is now given of the MHDF, which provides recursive suboptimal approximations of the minimum mean square error (MMSE) estimates. A detailed presentation of the filter can be found in [1].

Consider the class of stochastic discrete-time systems defined by the following models

$$\begin{aligned} x_{k+1} &= A_k x_k + v_k + w_k^s && \text{(state)} \\ y_k &= h_k(x_k) + w_k^m && \text{(measurement)} \end{aligned}$$

with $x, v, w^s \in \mathbb{R}^n$ and $y, w^m \in \mathbb{R}^q$; v_k is a deterministic input, while the noises w_k^s, w_k^m respectively affect the state transition and the measurement process at step k. Assume the following hypotheses are satisfied:

(H1) h_k is bounded and *piecewise-linear*, i.e., there exists a partition $\mathcal{Z}_k = \{Z_{k,j}\}_{j=1\ldots N_k}$ of $\mathbb{R}^n$ consisting of convex subsets (with nonzero lebesgue measure), such that for all j and $x \in Z_{k,j}$

$$h_k(x) = H_{k,j}\, x + \zeta_{k,j} \qquad \zeta_{k,j} \in \mathbb{R}^q,$$

with $H_{k,j}$ a $q \times n$ matrix (null on unbounded sets);

(H2) w_k^s, w_k^m are gaussian random variables with zero mean and covariances S_k, M_k, respectively;

(H3) x_0 is a gaussian random variable with mean value μ_0 and covariance C_0;

(H4) x_0, w_k^s, w_l^m are mutually independent for any k, l.

The MHDF algorithm consists in the iterated application of the *prediction* (PR_k) and *updating* (UP_k) endomorphisms, defined over the set of gaussian mixture densities. For the considered systems, the analytical description of such operators is derived as follows.

Denote by $\Phi_l(\cdot, C)$ the generic gaussian density over $\mathbb{R}^l$ with zero mean value and $l \times l$ covariance matrix C. Let Ψ_k be the gaussian mixture[1] representing the con-

[1] An upper bound on the number r_k of components of the mixture is given by N_k, i.e., the number of measurement hypotheses induced by the partition $\mathcal{Z}_k$ of the state space $\mathbb{R}^n$.

ditional density of the state x_k given the information $Y_k = \{y_1, \ldots, y_k\}$ at time step k:

$$\Psi_k(x_k) = \sum_{i=1}^{r_k} \lambda_{k,i} \Phi_n(x_k - \mu_{k,i}, C_{k,i})$$

with $\lambda_{k,i} \geq 0$ and $\sum_{i=1,\ldots,r_k} \lambda_{k,i} = 1$. The operator

$$\mathrm{PR}_k(\Psi_k)|_{x_{k+1}} = \sum_{i=1}^{r_k} \lambda_{k,i} \Phi_n(x - \hat{\mu}_{k+1,i}, P_{k,i})$$

with $\hat{\mu}_{k+1,i} = A_k \mu_{k,i} + v_k$ and $P_{k,i} = A_k C_{k,i} A_k^T + S_k$, predicts the conditional density of the state x_{k+1} given $Y_k = \{y_1, \ldots, y_k\}$, after the application of input v_k.

Given the new measurement y_{k+1}, operator UP_k is used to update the conditional density $\hat{\Psi}_k = \mathrm{PR}_k(\Psi_k)$, resulting in an approximation of the conditional density of x_{k+1} given $Y_{k+1} = \{y_1, \ldots, y_{k+1}\}$:

$$\mathrm{UP}_k(\hat{\Psi}_k)|_{x_{k+1}} = \sum_{j=1}^{N_{k+1}} \lambda_{k+1,j} \Phi_n(x_{k+1} - \mu_{k+1,j}, C_{k+1,j})$$

with the mixture parameters $\lambda_{k+1,j}$, $\mu_{k+1,j}$ and $C_{k+1,j}$ obtained as

$$\lambda_{k+1,j} = \frac{\gamma_j}{\sum_{p=1}^{N_{k+1}} \gamma_p}$$

$$\mu_{k+1,j} = \sum_{i=1}^{r_k} \frac{\nu_{i,j}}{\gamma_j} \int_{Z_{k+1,j}} z \Phi_n(z - \eta_{i,j}, D_{i,j}) dz$$

$$C_{k+1,j} = \sum_{i=1}^{r_k} \frac{\nu_{i,j}}{\gamma_j} \int_{Z_{k+1,j}} z z^T \Phi_n(z - \eta_{i,j}, D_{i,j}) dz - \mu_{k+1,j} \mu_{k+1,j}^T$$

with

$$\gamma_j = \sum_{i=1}^{r_k} \nu_{i,j} \int_{Z_{k+1,j}} \Phi_n(z - \eta_{i,j}, D_{i,j})\, dz$$

and

$$\begin{aligned}
\nu_{i,j} &= \lambda_{k,i} \Phi_q(y_{k+1} - H_{k+1,j} \hat{\mu}_{k+1,i} - \zeta_{k+1,j}, E_{i,j}) \\
\eta_{i,j} &= \hat{\mu}_{k+1,i} + K_{i,j}(y_{k+1} - H_{k+1,j} \hat{\mu}_{k+1,i} - \zeta_{k+1,j}) \\
D_{i,j} &= P_{k,i} - K_{i,j} E_{i,j} K_{i,j}^T \\
K_{i,j} &= P_{k,i} H_{k+1,j}^T E_{i,j}^{-1} \\
E_{i,j} &= H_{k+1,j} P_{k,i} H_{k+1,j}^T + M_{k+1}
\end{aligned}$$

for $i = 1, \ldots, r_k$ and $j = 1, \ldots, N_{k+1}$.

The above integral evaluations can be approximated via a Monte Carlo technique [2]. For example, consider the third integral

$$\int_{Z_{k+1,j}} z z^T \Phi_n(z - \mu_{i,j}, D_{i,j})\, dz.$$

A sequence of samples $z_1, \ldots, z_K$ drawn from the gaussian random variable $\Phi_n(\cdot, I)$ is needed. Letting $\bar{z} = L_{i,j}^{-1}(z + \mu_{i,j})$, where $L_{i,j}$ is the Cholesky factor of $D_{i,j}$, we obtain the sequence of draws $\bar{z}_1, \ldots, \bar{z}_K$ with distribution $\Phi_n(\cdot - \mu_{i,j}, D_{i,j})$. For any measurable function $z \mapsto F(z)$, such that the integral

$$\int_{\mathbb{R}^q} F(z)\, \Phi_n(z - \mu_{i,j}, D_{i,j})\, dz$$

exists, the Kolmogorov law of large numbers implies

$$\lim_{K \to \infty} \frac{1}{K} \sum_{t=1}^{K} F(\bar{z}_t) = \int_{\mathbb{R}^q} F(z)\, \Phi_q(z - \mu_{i,j}, D_{i,j})\, dz$$

almost surely [3]. Hence, for a sufficiently large K, we can use the following approximation

$$\frac{1}{K} \sum_{t=1}^{K} \bar{z}_t \bar{z}_t^T \Upsilon_{Z_{k+1,j}}(\bar{z}_t) \approx \int_{Z_{k+1,j}} z z^T\, \Phi_q(z - \mu_{i,j}, D_{i,j})\, dz,$$

being $\Upsilon_{Z_{k+1,j}}(\cdot)$ the *characteristic function* of $Z_{k+1,j}$:

$$\Upsilon_{Z_{k+1,j}}(\bar{z}_t) = \begin{cases} 1 & \bar{z}_t \in Z_{k+1,j} \\ 0 & \text{else.} \end{cases}$$

For the considered discrete-time systems satisfying (H1–H4), the operator UP_k provides a suboptimal approximation of MMSE estimates (see [1] for the proof).

3 Application to localization

Consider a robot with the kinematics of a unicycle. The generalized coordinate vector is $x \in \mathbb{R}^2 \times SO(1)$, with (x_1, x_2) the cartesian coordinates of the wheel axle midpoint and x_3 the robot orientation w.r.t. the horizontal axis of the world frame, as shown in Fig. 1. The kinematic model is

$$\begin{aligned}
\dot{x}_1 &= u_1 \cos x_3 \\
\dot{x}_2 &= u_1 \sin x_3 \\
\dot{x}_3 &= u_2,
\end{aligned} \tag{1}$$

with u_1, u_2 the driving and steering velocities.

3.1 State and measurement models

To derive an exact discrete-time system representing the sampled dynamics of eqs. (1), it is convenient to consider the following change of coordinates

$$\begin{aligned}
\xi_1 &= x_3 \\
\xi_2 &= x_1 \cos x_3 + x_2 \sin x_3 \\
\xi_3 &= x_2 \cos x_3 - x_1 \sin x_3
\end{aligned} \tag{2}$$

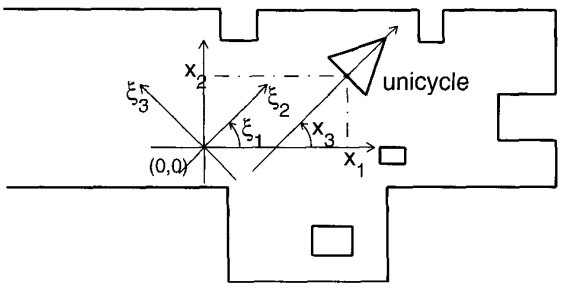

Figure 1: Environment and unicycle-like mobile robot

and input transformation

$$\begin{aligned} v_1 &= u_1 + (x_2 \cos x_3 - x_1 \sin x_3)u_2 \\ v_2 &= u_2. \end{aligned}$$

Coordinate ξ_1 is the robot orientation, while (ξ_2, ξ_3) measure its position in a *moving frame* rotated by the angle x_3 w.r.t. the world frame, so as to align the ξ_2 axis with the robot forward direction (see Fig. 1). In the ξ coordinates, the system is in chained form [4]:

$$\begin{aligned} \dot{\xi}_1 &= v_1 \\ \dot{\xi}_2 &= v_2 \\ \dot{\xi}_3 &= \xi_2 v_1. \end{aligned} \tag{3}$$

Under the assumption of digital control implementation, u_1 and u_2 assume constant values $u_{1,k}$ and $u_{2,k}$, respectively, in the sampling interval $[kT, (k+1)T]$. Letting $\xi_k = \xi(kT)$, integration of eqs. (3) yields the following exact sampled dynamics [5]:

$$\xi_{k+1} = A_k \xi_k + v_k, \tag{4}$$

with

$$A_k = \begin{pmatrix} 1 & 0 & 0 \\ 0 & \cos(Tu_{2,k}) & \sin(Tu_{2,k}) \\ 0 & -\sin(Tu_{2,k}) & \cos(Tu_{2,k}) \end{pmatrix}$$

$$v_k = \begin{pmatrix} Tu_{2,k} \\ u_{1,k} \frac{\sin u_{2,k}}{u_{2,k}} \\ u_{1,k} \frac{\cos u_{2,k} - 1}{u_{2,k}} \end{pmatrix}.$$

Equation (4) is a linear (in the state ξ) discrete-time system that, given the control inputs $u_{1,k}$ and $u_{2,k}$, allows to compute the robot coordinates $\xi_k + 1$ at the next sampling instant. By inverting eqs. (2) it is then possible to obtain the world coordinates x.

Assume now that the obstacle-free region is a compact connected set $\mathcal{M} \subset \mathbb{R}^2$, whose boundary $\partial\mathcal{M}$ is a finite collection of segments, as shown for example in Fig. 1. The robot is equipped with q range finders, oriented at angles $\theta_1, \ldots, \theta_q$ w.r.t. the ξ_2 axis; w.l.o.g., the sensors are supposed to be pointwise and placed exactly at the wheel axle midpoint. Let

$$x_p = \begin{pmatrix} x_1 \\ x_2 \end{pmatrix} \qquad \xi_p = \begin{pmatrix} \xi_2 \\ \xi_3 \end{pmatrix}$$

denote the positional part of vectors x and ξ, respectively. From eqs. (2) we have

$$x_p = R(\xi_1)\xi_p,$$

with $R(\xi_1)$ the rotation matrix

$$R(\xi_1) = \begin{pmatrix} \cos\xi_1 & -\sin\xi_1 \\ \sin\xi_1 & \cos\xi_1 \end{pmatrix}.$$

In the world frame coordinates x, the i-th component of the measurement function $h^x \in \mathbb{R}^q$, which models the i-th range finder, is defined as

$$h_i^x(x) = \min_{q \in Q_i(x)} ||x_p - q||,$$

where

$$Q_i(x) = r(x_p, x_3 + \theta_i) \cap \partial\mathcal{M}$$

is the set of points where the boundary $\partial\mathcal{M}$ intersects the range finder axis, i.e., the half-line $r(x_p, x_3 + \theta_i)$ with origin x_p and orientation $x_3 + \theta_i$. As $\partial\mathcal{M}$ consists of segments, h^x is piecewise-linear w.r.t. x_p.

In the ξ coordinates, the i-th component of the measurement function $h^\xi \in \mathbb{R}^q$ takes the form

$$h_i^\xi(\xi) = \begin{cases} h_i^x(R(\xi_1)\xi_p, \xi_1) & \text{if } R(\xi_1)\xi_p \in \mathcal{M} \\ d_\infty & \text{otherwise.} \end{cases} \tag{5}$$

Note that the domain of h^ξ has been extended to the whole ξ space (including configurations that do not map back to collision-free robot positions) by means of a suitable constant $d_\infty < 0$. Since the transformation between x_p and ξ_p is linear, also function h^ξ (including the extension) is piecewise-linear w.r.t. ξ_p; however, due to the presence of the rotation matrix $R(\xi_1)$, h^ξ is *not* piecewise-linear w.r.t ξ_1.

An unfortunate consequence of the essential nonlinearity of the measurement model (5) in ξ_1 is that the MHDF algorithm cannot be used for state estimation, because its working hypothesis (H1) is violated. To overcome this difficulty, we suppose here that the robot is also equipped with a heading sensory system, which provides an accurate estimate of the orientation angle. This is exactly the case of our experimental platform,

the ATRV-Jr mobile robot (see Sect. 4). Techniques for orientation estimation are presented[2] in [6] and [7].

Wrapping up, our state and (augmented) measurement model are respectively represented by eq. (4) and

$$y_k = \begin{pmatrix} y_{1,k} \\ y_{h,k} \end{pmatrix} = \begin{pmatrix} \xi_{1,k} \\ h^{\xi}(\xi_k) \end{pmatrix}, \tag{6}$$

with $y_{1,k} \in I\!R$ and $y_{h,k} \in I\!R^q$.

3.2 Perturbed models

As usual, perturbed versions of the state and measurement model are considered to account for system perturbations as well as measuring uncertainties.

The kinematic model (4) is derived under the assumption of rolling without slipping. This ideal condition is often violated in practical operation, so that it is necessary to consider the perturbed state model

$$\xi_{k+1} = A_k \xi_k + v_k + w_k^s, \tag{7}$$

with w_k^s the state transition noise. Using the partition of ξ, and letting $A_{p,k} = R^T(T\omega_{2,k})$, eq. (7) becomes

$$\begin{pmatrix} \xi_{1,k+1} \\ \xi_{p,k+1} \end{pmatrix} = \begin{pmatrix} 1 & 0 \\ 0 & A_{p,k} \end{pmatrix} \begin{pmatrix} \xi_{1,k} \\ \xi_{p,k} \end{pmatrix} + \begin{pmatrix} v_{1,k} \\ v_{p,k} \end{pmatrix} + \begin{pmatrix} w_{1,k}^s \\ w_{p,k}^s \end{pmatrix},$$

with similar partitions for v_k and w_k^s. The perturbed measurement model is derived from (6) as

$$y_k = \begin{pmatrix} y_{1,k} \\ y_{h,k} \end{pmatrix} = \begin{pmatrix} \xi_{1,k} \\ h^{\xi}(\xi_k) \end{pmatrix} + \begin{pmatrix} w_{1,k}^m \\ w_{h,k}^m \end{pmatrix},$$

being $w_{1,k}^m$ and $w_{h,k}^m$ the noises affecting the measures of orientation and distances, respectively.

If the heading measure $y_{1,k}$ is sufficiently accurate (i.e., if $w_{1,k}^m \approx 0$), we can obtain a *reduced* state and measurement model (including perturbations) as

$$\xi_{p,k+1} = A_{p,k}\xi_{p,k} + v_{p,k} + w_{p,k}^s \tag{8}$$

$$y_{h,k} = h^{\xi}(y_{1,k}, \xi_{p,k}) + w_{h,k}^m, \tag{9}$$

in which $y_{1,k} = \xi_{1,k}$ acts as an input vector.

It is clear that system (8–9) belongs to the class of stochastic discrete-time systems considered in Sect. 2. Moreover, the measurement function $h_k(\xi_{p,k}) = h^{\xi}(y_{1,k}, \xi_{p,k})$ is piecewise-linear in the state $\xi_{p,k}$. Hence, if also hypotheses (H2–H4) on the stochastic nature of the models are satisfied, the MHDF can be applied to the state estimation problem for system (8–9).

[2] In particular, in [6] it is proposed a method which provides high-performance heading estimation without recurring to an interaction model of the robot and the environment. This approach, based on gyro modeling, combines inertial navigation with absolute measurements.

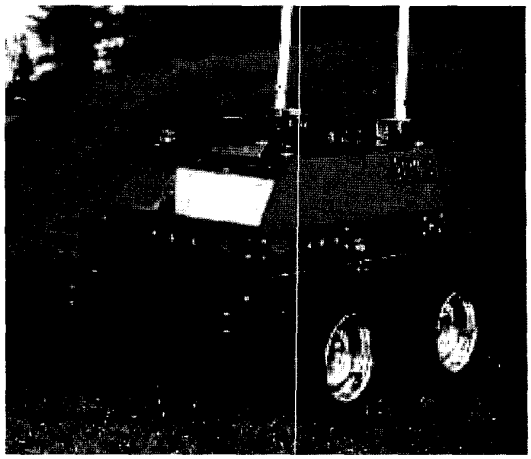

Figure 2: The ATRV-Jr mobile robot

4 Experimental results

Figure 2 shows the ATRV-Jr by Real World Interface, the mobile robot used in our experiments. This vehicle, mainly designed for outdoor applications and research, has a four-wheel drive, differentially steered locomotion system. Its sensory equipment includes two optical encoders measuring the wheel rotation, an inertial platform and a 180° degrees laser scanner oriented in the forward direction. A peculiarity of the ATRV-Jr is the built-in odometry: although the encoders are not directly accessible, a low-level module provides the position estimate as reconstructed from the encoders.

Our localization system considers a sensory model with 5 range measures (chosen among the set of 181 measures provided by the laser scanner) and a heading estimate derived by integration of the angular velocity measure given by the inertial platform. The built-in odometry allows us to compute directly the ATRV-Jr kinematics whose perturbed model has the form (8).

Experiments have been carried out in an office-like indoor environment whose 2D map is shown in Fig. 1. We have collected the data of a dozen of ATRV-Jr runs with different initial positions and paths, so as to explore the obstacle-free region. All runs have been performed at a velocity of approximately 0.1 m/s, resulting in an average traveling time of 1 min. The laser data and the (built-in) odometric estimate have been sampled at a frequency of 1 Hz. To provide our localization system with a sufficiently accurate heading estimate, the angular velocity has been sampled instead at 10 Hz; thanks to the low velocity and the relatively short traveling time, such a frequency has guaranteed an orientation error lower than 2°.

To assess the localization performance of the MHDF versus the classical EKF, we have adopted a mixed approach. The collected experimental data (i.e., control inputs, laser range measures and heading estimates) have been used in a Monte Carlo simulation setting by introducing an artificial uncertainty on the robot initial position. This uncertainty has been chosen as a zero mean gaussian noise with RMS deviation of 0.5 m. For each set of experimental data we have obtained a set of realizations of EKF and MHDF estimates by sampling 100 draws from the initial noise. Then, we have compared these estimates with the true robot positions using the criteria of root mean square error (RMSE), maximum error (MaxError) and estimate dispersion (DISP), defined as follows:

$$\begin{aligned} \mathrm{RMSE}_k &= < \|\xi^i_{p,k} - \hat{\xi}^i_{p,k}\|^2 >^{\frac{1}{2}} \\ \mathrm{MaxError}_k &= \max_{i=1,\ldots,M} \|\xi^i_{p,k} - \hat{\xi}\| \\ \mathrm{DISP}_k &= < \|(\xi^i_{p,k})_i - < (\xi^i_{p,k})_i > \| >^{\frac{1}{2}} . \end{aligned}$$

Here, $\xi^i_{p,k}$ and $\hat{\xi}^i_{p,k}$ are respectively the position and its estimate at time-step k in the i-th realization, and the angle brackets indicate the mean value of the considered sequences w.r.t. the i index.

We report here the plots of RMSE_k, $\mathrm{MaxError}_k$ and DISP_k for one of the experiments. These plots, shown in Figs. 5, 6 and 7, show that the MHDF estimates rapidly converge to the real robot position with a very low dispersion. Furthermore, the behavior of the maximum estimation error shows that the MHDF estimates are rather robust w.r.t. the *a priori* position knowledge. On the contrary, the EKF estimates are unreliable in terms of both accuracy and dispersion and, as a consequence, much less robust.

To better illustrate this fact, it is useful to analyze two realizations taken from two typical experiments. The results are reported in Figs. 3–4 in terms of true robot positions and estimates provided by the EKF and the MHDF. In both cases it appears clearly that the EKF estimates are unreliable, whereas the MHDF estimates are remarkably precise.

5 Conclusions

The localization problem has been addressed for a robot with unicycle kinematics and equipped with range finders, moving in environments with nonsmooth geometry, i.e., whose obstacle-free region has a piecewise-linear boundary. A novel solution has been presented based on a multi-modal filter called Multi-Hypothesis Density Filter. The performance of the MHDF has been compared in terms of BIAS and RMSE to that of the EKF, through a series of Monte Carlo experiments. The results have shown that the EKF estimates computed for certain realizations of the stochastic process may become unreliable, whereas the MHDF provides better estimates on the average.

The superior performance of the MHDF (which we have also observed through extensive simulation campaigns [8]) has a price in terms of computational load. At the present stage of our study, a single step of the MHDF is 30 or 40 times slower than a single step of the EKF, essentially due to the heavy cost of building the partition $\mathcal{Z}_k$ [1]. One way to reduce the complexity is to obtain $\mathcal{Z}_k$ by updating $\mathcal{Z}_{k-1}$ only in the area where the predicted probability density of the robot position differs significantly from zero.

Finally, it is worth to mention another possible applications of the MHDF to sensor fusion. It has been shown here that the measurement function modeling a range finder can be reduced, under certain hypotheses, to a piecewise-linear function. Another type of sensor that admits piecewise-linear measurement models are proximity sensors. For instance, consider a bumper ring placed all around the robot. Its measures are inherently boolean (on/off), and therefore can be modeled by characteristic functions over suitable neighborhoods of $\partial\mathcal{M}$. This type of function is clearly piecewise-linear and bounded. Since this function is generally constant, the EKF algorithm cannot take advantage of such measures, whereas the MHDF algorithm would be able to process them in order to improve the estimation.

6 Acknowledgments

We thank Prof. G. Ulivi of Università di Roma Tre for allowing us to perform experiments on ATRV-Jr.

References

[1] F. M. Antoniali, *A novel bayesian approach to mobile robot localization*, PhD thesis, Dipartimento di Informatica e Sistemistica, Università degli Studi di Roma "La Sapienza", December 2000.

[2] J. Geweke, "Monte carlo simulation and numerical integration", in *Handbook of Computational Economics*, H. M. Ammand, D. A. Kendrick, and J. Rust, Eds., pp. 731–800. Elsevier, 1996.

[3] C.W. Burill, *Measure, Integration, and Probability*, McGraw-Hill, 1972.

[4] R.M. Murray and S.S. Sastry, "Nonholonomic motion planning: Steering using sinusoids", *IEEE Trans. on Automatic Control,*, vol. 38, no. 5, pp. 700–716, 1993.

[5] E. Fabrizi, G. Oriolo, S. Panzieri, and G. Ulivi, "A kf-based localization algorithm for nonholonomic mobile

robots", in *Proc. 6th Mediterranean Conf. of Control and Automation*, Alghero, I, 1998, pp. 130–136.

[6] S.I. Roumeliotis, G.S. Sukhatme, and G.A. Bekey, "Circumventing dynamic modeling: Evaluation of the error-state kalman filter applied to mobile robot localization", in *Proc. 1999 IEEE Int. Conf. on Robotics and Automation*, Detroit, MI, 1999, pp. 1656–1663.

[7] B. Barshan and H.F. Durrant-Whyte, "Inertial navigation systems for mobile robots", *IEEE Trans. on Robotics and Automation,*, vol. 11, no. 3, pp. 328–342, 1995.

[8] F. M. Antoniali and G. Oriolo, "Localization of mobile robots in environments with non-smooth geometry", in *Proc. 6th IFAC Symp. on Robot Control*, Vienna, A, 2000.

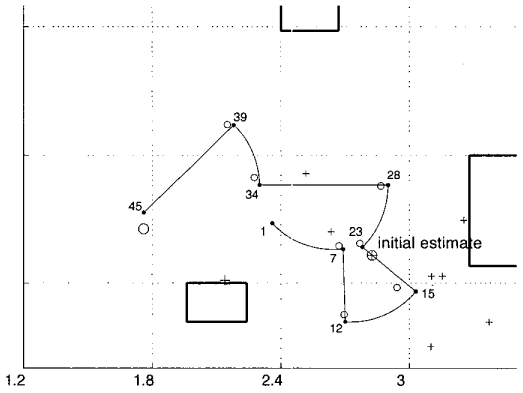

Figure 3: A realization of experiment 1: true robot positions (·), MHDF (○) and EKF (+) position estimates

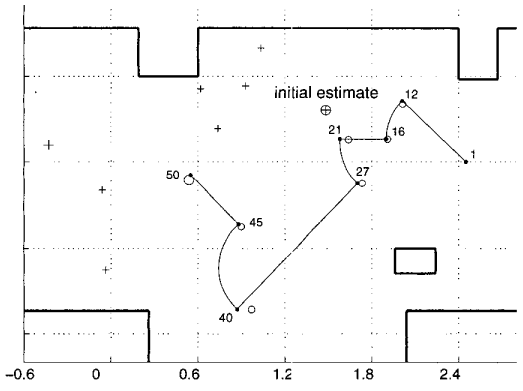

Figure 4: A realization of experiment 2: true robot positions (·), MHDF (○) and EKF (+) position estimates

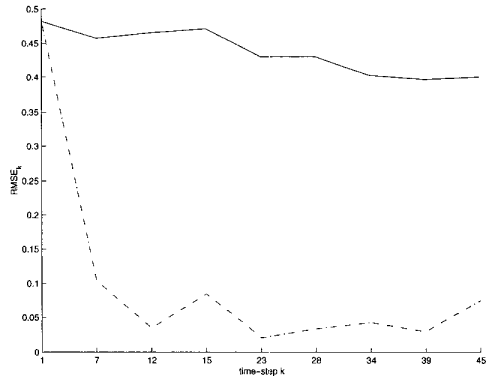

Figure 5: RMSE_k for MHDF (−·) and EKF (–)

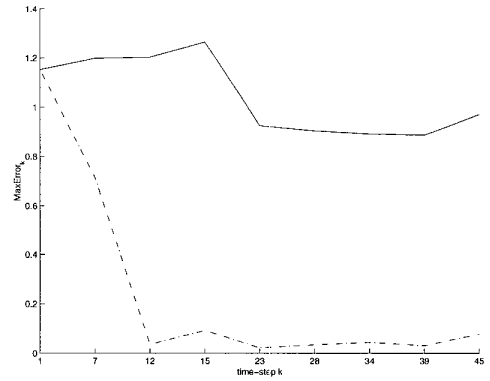

Figure 6: $\mathrm{MaxError}_k$ for MHDF (−·) and EKF (–)

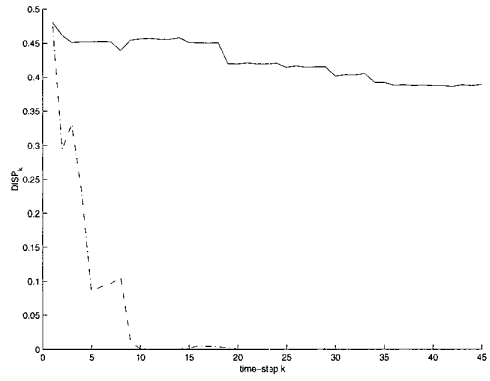

Figure 7: DISP_k for MHDF (−·) and EKF (–)